Flexural and compressive creep behavior of UHPFRC specimens

A. Llano-Torre[1], J.R. Martí-Vargas[1]*, and P. Serna[1]

[1]**ICITECH, Institute of Concrete Science and Technology, Universitat Politècnica de València, Valencia, Spain**

e-mail: aillator@upv.es; jrmarti@cst.upv.es; pserna@cst.upv.es;
*Corresponding author: Tel.: +34 96 3877007 (ext. 75612); Fax: +34 96 3877569;
e-mail address: jrmarti@cst.upv.es (José R. Martí-Vargas)
ICITECH, Universitat Politècnica de València, Building 4N, Camino de Vera s/n, 46022, Valencia, Spain

HIGHLIGHTS:
Flexural creep behavior of cracked UHPFRC is analyzed in service conditions.
Two different UHPFRC specimen sizes and shapes are considered.
Measurements from three experimental sources are considered.
Creep coefficients and parameters related with deferred deformations velocity are obtained.
A secondary creep stage is achieved after seven months of sustained loading.

LIST OF NOTATION:

(Note: the order is not strictly alphabetical to be more consistent by groups of parameters)

CMOD	crack mouth opening displacement
$CMOD_p$	maximum CMOD reached in the pre-cracking process
$CMOD_{ci}$	instantaneous CMOD at loading in the flexural creep period
$CMOD_{cd}{}^{j}$	deferred CMOD ─obtained from the measured value by adding the shrinkage effect along the instrumented base length─ after j days under sustained load in the flexural creep period
$CMOD_{ct}{}^{j}$	total CMOD after j days in the creep period ($CMOD_{ci}$ + $CMOD_{cd}{}^{j}$)
COR^{j-k}	crack opening rate between j and k days under sustained load in the flexural creep period
CS	maximum concrete compressive strain in a section under flexure
CS_{ci}	instantaneous CS at loading in the flexural creep period
$CS_{cd}{}^{j}$	deferred CS after j days under sustained load in the flexural creep period, obtained as the measured value minus $\varepsilon_{cs}{}^{j}$
$CS_{ct}{}^{j}$	total CS due to load after j days under sustained load in the flexural creep period (CS_{ci} + $CS_{cd}{}^{j}$)
CSR^{j-k}	compressive strain rate between j and k days under sustained load in the flexural creep period
f_c	concrete compressive strength at 28 days
f_L	limit of proportionality
$f_{R,1}$	residual flexural tensile strength corresponding to $CMOD_1$ = 0.5 mm
$f_{R,2}$	residual flexural tensile strength corresponding to $CMOD_2$ = 1.5 mm
$f_{R,3}$	residual flexural tensile strength corresponding to $CMOD_3$ = 2.5 mm
$f_{R,4}$	residual flexural tensile strength corresponding to $CMOD_4$ = 3.5 mm
$f_{R,p}$	residual flexural tensile strength at $CMOD_p$
$f_{R,c}$	applied stress during the creep period, in MPa
I_c	applied creep index, or applied stress level as percentage of $f_{R,p}$ ($I_c = f_{R,c} / f_{R,p}$)
ε_c	concrete compressive strain
$\varepsilon_{cs}{}^{j}$	concrete shrinkage strain at time j
ε_{ci}	instantaneous ε_c at loading in compression
$\varepsilon_{cd}{}^{j}$	deferred ε_c after j days under sustained load in compression, obtained as the measured value minus $\varepsilon_{cs}{}^{j}$
$\varepsilon_{ct}{}^{j}$	total ε_c due to load after j days under sustained load in compression (ε_{ci} + $\varepsilon_{cd}{}^{j}$)
CR^{j-k}	compressive strain rate between j and k days under sustained load in compressive creep test
φ^{j}	creep coefficient at j days in compression
$\varphi_{CMOD,c}{}^{j}$	creep coefficient at j days obtained from CMOD measurements
$\varphi_{CS,c}{}^{j}$	creep coefficient at j days obtained from compressive strain measurements in the flexural creep period

ABSTRACT

The long term behavior of Ultra High Performance Fiber Reinforced Concrete (UHPFRC) is analyzed in this study. The experimental campaign covered creep in compression and creep in flexure in cracked state. Three types of specimens were cast: cylindrical specimens (Ø100x200mm) for compressive creep and shrinkage, and prismatic specimens type regular "R" (150x150x600mm) and type slim "S" (150x40x600mm) for flexural creep in cracked state. Specimens R were notched up to 50mm in depth to weak the central section and then pre-cracked until 0.65mm of Crack Mouth Opening Displacement (CMOD). Specimens S

were pre-cracked unnotched until a loss of 50% of stiffness was observed. Flexural creep tests were performed during 270 days under load, and until 360 days the compressive tests. Measurements from three experimental sources were obtained: CMOD, compressive strains on top of prismatic specimens and longitudinal compressive strains in cylindrical specimens. Creep coefficients and parameters related with deferred deformations velocity were obtained from all three sources. Creep coefficients under flexure at 270 days ranged from 0.62 to 1.20 in the tensile zone, and from 0.72 to 0.90 in the compressive zone. Creep coefficient in compression at one year was 1.07, which is consistent with values found in the literature. Deferred deformations velocities at early ages were greater in specimens R than in specimens S, and a secondary creep stage was achieved in all specimens after 210 days of sustained loading.

KEYWORDS: Ultra-High Performance Fiber Reinforced Concrete; UHPFRC; steel fiber; creep; long-term; bending; compression

1. INTRODUCTION

Ultra-High Performance Concrete (UHPC) is a cementitious, concrete material that has a minimum specified compressive strength of 120 MPa [1]. The UHPC designation was first used in 1994 [2] to refer to an optimized particle-packing material, which previously was known as reactive-powder concrete since it contained very fine materials [3,4]. Fibers are generally included in the mixture to achieve specified requirements for UHPC; in that case, the resulting concrete is called Ultra-High Performance Fiber Reinforced Concrete (UHPFRC) which, in turn, can be also considered a special type of High Performance Fiber Reinforced CementitiousComposite (HPFRCC) [5].

Technologies on which UHPFRC is based are well-known. Although the number of UHPFRC applications is increasing [6-10], its use is focused on few singular structures around the world. This is due to the lack of knowledge and suitable codes for design, and also to the associated high costs of the concrete constituent materials [10,11]. Therefore, it is necessary to advance in a deep knowledge of mechanical behavior of UHPFRC.

Recent documents summarize information about the various mechanical properties that are relevant to the structural design of UHPFRC [12]: compressive strength, tensile strength, modulus of elasticity, poisson's ratio, fatigue behavior, thermal properties, bond strength, impact resistance, creep and shrinkage. Some recent advances in knowledge on these properties have been achieved [13-19]. However, research on creep of UHPFRC is still scarce and has mainly been focused in creep under compression [12,20].

Compressive creep of UHPFRC is mainly of interest for prestressed applications. The rapid achievement of strength at early age together with the high shrinkage of UHPFRC, require that structural design of UHPFRC elements must take into account delayed deformations. The date of loading, duration of the applied stress and whether a heat treatment is applied are the main parameters that influence the compressive creep behavior of UHPFRC. According to AFGC [21], after heat treatment is applied, creep is not dependent on the date of loading. The most common heat treatment applied to UHPFRC consist on taking the UHPFRC members to a relatively high level of temperature (around 90ºC) and to moisture content close to saturation a few hours after the concrete has been set. However, this type of cure treatment is

not easy to apply in large elements and it may be an expensive procedure. Most of UHPFRC civil engineering applications use a standard cure regime. In this case, the date of loading has a significant influence on the creep behavior, which is considered in detail in AFGC [21] as shown in Table 1. Creep coefficients proposed in FHWA [12], as well as those proposed in JSCE [22] and Australian recommendations [23], and by Graybeal [24], are also included in Table 1.

Table 1. Creep coefficients for UHPFRC in compression.

Recommendations	Cure regime	Date of loading	Final creep coefficient
FWHA (2013) [6]	Heat Treatment	-	0.20 – 0.80
AFGC (2013) [7]	Standard	1	2.27
	Standard	4	1.80
	Standard	7	1.57
	Standard	28	1.08
	Heat Treatment	-	0.30
JSCE (2006) [22]	Standard	-	1.20
	Heat Treatment	-	0.40
Australia (2000) [23]	Standard	4	1.80
	Standard	28	1.20
	Heat Treatment	4	0.50
	Heat Treatment	28	0.30
Graybeal (2006) [24]	Standard	28	0.78*
	Heat Treatment	4	0.30*

**Creep coefficient at one year of loading*

The ductile behavior of UHPFRC is a first for concrete, with the capacity to deform and support flexural loads, even after initial cracking. The fiber reinforcement serves to resist tensile stresses once tensile cracking of the UHPFRC matrix occurs. Therefore, the post-cracking mechanical response of UHPFRC is of crucial importance in applications in which the high performance of UHPFRC makes possible to design eliminating the need of reinforcing bars. The absence of that reinforcement makes essential the understanding of the UHPFRC long-term behavior in the cracked state under service conditions. However, there is no mention about it in any current design code or international recommendations [25].

Regarding creep of UHPFRC in cracked state, a few studies have been carried out. Some of them have been focused on creep in tension, but only for short-term [26-28] and emphasizing the importance of further studies [29,30], and there are results from only three studies [31-33] related to flexural creep of UHPFRC in cracked state. A short term high sustained load was considered, without a clear stabilization of measurements within 27 h [31]; after 30 days at a sustained applied load of 35% of the load at which the first crack appeared, creep coefficients ranging from 0.63 to 1.08 where obtained when steel fibers were used, whereas and 1.27 to 1.67 for the case of glass fibers [32]; and a creep coefficient below 0.3 was obtained at 28 days under a sustained load of 50% of the pre-cracking load in specimens combining short and long steel fibers [33].

Therefore, knowledge on flexural creep behavior of UHPFRC in the cracked state still constitutes a field to be explored and a challenge for researchers. For this reason, the objective

of the study presented in this paper is to analyze the long term flexural creep behavior of an UHPFRC. Notched and unnotched prismatic specimens were included in the experimental program, as well as cylindrical specimens aimed to obtain and compare results considering compressive creep and shrinkage.

It should be noted that a standard thermal cure was applied to specimens, which led to an average concrete compressive strength of 117.6 MPa at 28 days. In this way, the analyzed specimens represent an interesting starting point for further studies since the creep is analyzed in an unfavorable situation for UHPFRC: standard thermal cure and minimum compressive strength.

2. EXPERIMENTAL PROGRAM

An experimental campaign was carried out to cover the desired aspects regarding the long term behavior of UHPFRC specimens. The designed matrix, the steel fibers used and test specimens are described.

2.1. Concrete matrix composition

Based on previous experiences in real applications [10], one UHPFRC matrix was designed. The cement used in the matrix composition was CEM I 42.5-SR 5 [34], to avoid an excessive heat of hydration, and the water-to-cement ratio (w/c) adopted was 0.22. The aggregates were composed by two different sizes of siliceous sand, with a maximum aggregate size of 1.5 mm. The silica fume was undensified (Elkem Microsilica 940U), and the superplasticizer was policarboxileter based and was dosed in high ratio to introduce a great workability. Table 2 shows the dosage of each component in kg/m^3.

Table 2. Concrete mix design.

Component	**Dosage (kg/m^3)**
CEM I 42.5-SR 5	900
Water	195
Sand 1 (0.13-0.80 mm)	310
Sand 2 (0.6-1.2 mm)	576
Silica fume	225
Superplasticizer	30
OL 13/0.20	80
Dramix RC 80/30 BP	80

As the concrete was designed to work without any other reinforcement than fibers, two types of steel fibers were used, which are shown in Fig. 1, both of them with a high tensile strength. Based on the different ability of the fibers to provide crack bridging forces across the concrete cracked sections, the shortest fibers (OL 13/0.20) control the micro-cracking, whereas the longest fibers (Dramix RC 80/30 BP) control the macro-crack propagation to improve ductility. The UHPFRC was reinforced with 160 kg/m^3 of steel fibers. The fiber dosage was composed by a mix of 50% of both fibers: 80 kg/m^3 of each fiber type. The main characteristics and properties of the used fibers are shown in Table 3.

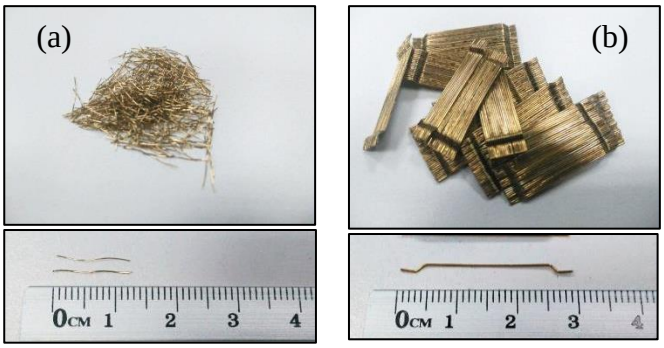

Figure 1. Fibers used: (a) OL 13/0,20, and (b) Dramix RC 80/30 BP.

Table 3. Properties of fibers.

Properties	OL 13/0.20	Dramix RC 80/30 BP
Fiber length (L)	13	30
Wire diameter (d)	0.20	0.38
Aspect ratio (L/d)	65	79
Tensile strength [MPa]	2,600	3,070
Young's Modulus [GPa]	210	200

2.2. Test specimens

Specimens with different shapes were used, as follows: (a) regular ("R") prismatic specimens, to be tested in bending notched and pre-cracked; (b) slim ("S") prismatic specimens, to be tested in bending pre-cracked but unnotched; and (c) cylindrical specimens, to be tested in compression.

Specimens were cast from three batches of the same UHPFRC mix to cover all requirements of testing methodologies, including characterization tests (compression and bending) and long term tests (flexural creep in cracked state, compressive creep and shrinkage).

In order to perform the compressive strength characterization and the compressive creep test, 8 cylindrical specimens of dimensions Ø100x200mm were cast. This size was adopted due to limitations in load capacity of the frames for compressive creep tests, which required a specific stress level to be applied.

To characterize the flexural behavior and to perform the flexural creep tests, 6 type R specimens of 150x150x600mm (as defined in EN14651:2007 [35]) and 6 type S specimens 150x40x600mm were cast. These particular slim specimens served to check flexural creep behavior in slender UHPFRC elements. Three specimens of each shape were tested for characterization purposes and three for flexural creep tests. For type R specimens, a 50 mm depth notch was sawed (instead of 25 mm as specified in EN14651:2007 [35]) with the aim of weak the central section of the specimens. The notch was 3 mm thick, which was less than the maximum of 5 mm specified in [35]. This extra-large notch was required to ensure the appearance of cracks only at the notch tip..

It is important to highlight that in the flexural test there are two different zones involved in the equilibrium: tensile and compressive. For this reason, in all specimens, a Linear Variable Differential Transformer (LVDT) was located below the specimen to measure the Crack

Mouth Opening Displacement (CMOD) in the tensile zone, whereas centered on the top surface of each specimen, a strain gauge was located to measure the maximum concrete compressive strain (CS) in the compressed zone. Fig. 2 shows the dimensions of the specimens for flexural tests, as well as the load configuration and the location of measurement devices.

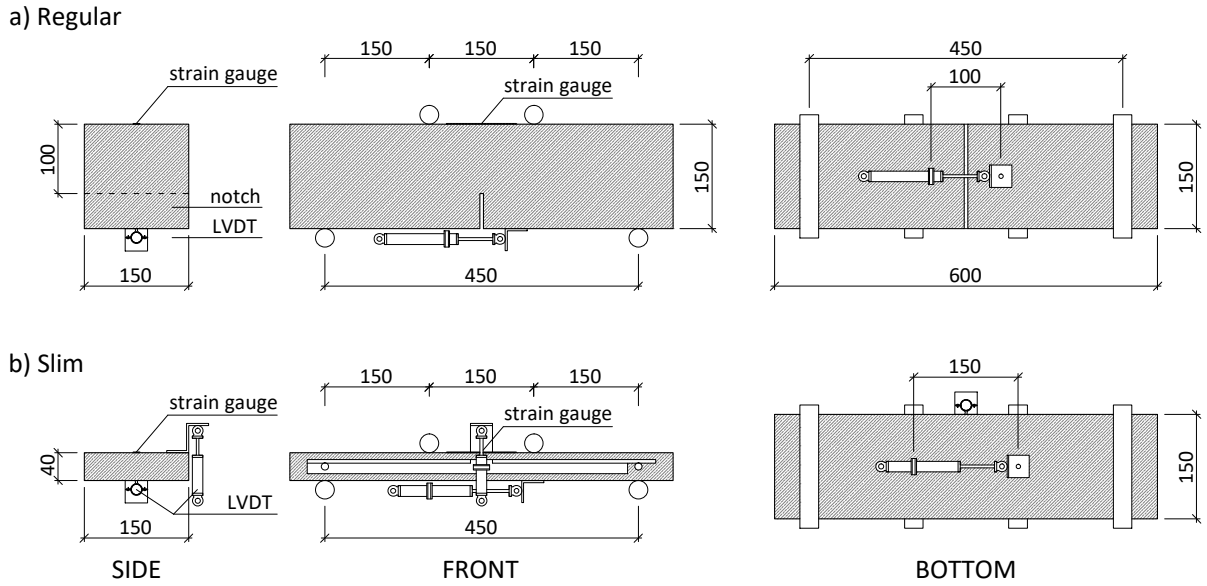

Figure 2. Dimensions of specimens, instrumentation and load configuration for flexural creep tests: (a) regular specimens, and (b) slim specimens.

2.3. Test parameters

All specimens were tested at 28 days after casting and curing in a chamber under standard conditions. The stress level chosen to be applied for compressive creep test was 40% of f_c. For the flexural creep tests, the main parameters were: (a) the initial CMOD (maximum CMOD reached in the pre-cracking process ─$CMOD_p$─), as an initial damage level by pre-cracking; and (b) the applied creep index (I_c) or stress level applied during creep test (defined in this study as percentage of the residual flexural tensile strength at $CMOD_p$ ─$f_{R,p}$─).

Regarding flexural creep tests, there were some differences in the determination of $CMOD_p$ depending on the specimen type (R or S): (a) in case of type R specimens, the desired initial damage corresponded to a $CMOD_p$ of 0.65 mm; and (b) in case of type S specimens, the desired initial damage corresponded to a loss of half the stiffness. For both types of specimens, the adopted I_c was 50% and hence the subsequent applied stress during the creep period ─$f_{R,c}$─ was $0.5 \cdot f_{R,p}$.

It should be noted that, since the UHPFRC is highly reinforced, the crack propagation is rather different than in the conventional Fiber Reinforced Concrete (FRC). Instead of a unique crack located at the midspan, a high number of micro-cracks appears distributed between the loading points (see Fig. 3), which corresponds to the third central portion of the specimens in this case. Therefore, the CMOD registered during tests represents the total addition of all the micro-cracks openings. From the LVDT measurements, the CMOD was calculated as established in EN14651:2007 [35]. Although type S specimens are not standard sized specimens, the CMOD parameter was also calculated as reference parameter.

(a) (b)

Figure 3. Micro-crack patterns in UHPFRC specimens: (a) regular specimens, and (b) slim specimens.

3. TESTING METHODOLOGIES

3.1. Characterization tests

Concrete compressive strength was determined according to EN 12390-3:2009 [36] procedure. Flexural tensile strength was determined according to EN 14651:2007 [35], even though the shape and conditions of specimens were different.

3.2. Flexural creep tests

Flexural creep test in cracked state were scheduled with duration of 270 days. The test procedure followed a sequence of two main stages for each test specimen: pre-cracking and creep period. The first stage aims to pre-crack the specimen up to the desired crack opening or damage level (a four-point bending test configuration was used due to the location of one strain gauge on the center top of the specimen). In the second stage, a sustained load is applied on the specimens for a certain period of time in which deferred deformations occur (a four point bending test configuration was used to make more stable the column of specimens and uniformize micro-crack distribution). For a better understanding, Fig. 4 shows an idealized "stress - crack opening" diagram for a specimen including test stages as followed in other recent studies carried out on conventional FRC [37-40].

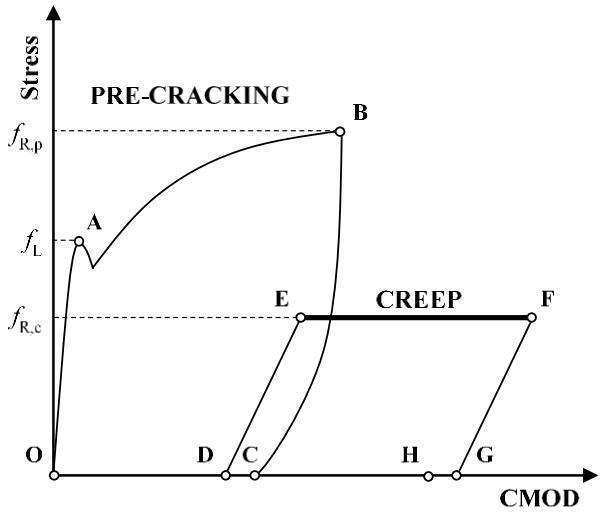

Figure 4. Idealized diagram of the main stages of a flexural creep test in cracked state.

In Fig. 4, the first part of the diagram corresponds to the pre-cracking stage. The curve begins at zero with an ascending linear branch until the first crack occurs (A, which corresponds to the limit of proportionality ─f_L─). After this, the test specimen is gradually loaded until the pre-cracking load value previously defined is reached (B, which corresponds to $CMOD_p$). Then the specimen is unloaded: the descending branch BC is developed during the unloading process, whereas the branch CD corresponds to the CMOD recovery during a stabilization period of 10 minutes after unloading. Point D serves as reference to the origin of deformations when the curve obtained in the flexural creep test (second stage) is added to the corresponding pre-cracking curve (first stage).

Also in Fig. 4, the second part of the diagram corresponds to the creep period, which starts with an ascending branch corresponding to the loading process (DE, in which the instantaneous CMOD at loading in the creep period ─$CMOD_{ci}$─ is developed). Then follows a horizontal branch (EF) where applied load is kept constant over time: the applied stress is $f_{R,c}$ and the deferred CMOD ─$CMOD_{cd}{}^{j}$─ are developed. The creep period ends up when the test specimen is unloaded. A new descending branch (FG) describes the post-creep unloading, and then the subsequent recovery (GH).

Following the exposed test methodology and using the testing frames available at ICITECH, the UHPFRC specimens were placed in a multiple-specimen setup, as shown in Fig. 5.

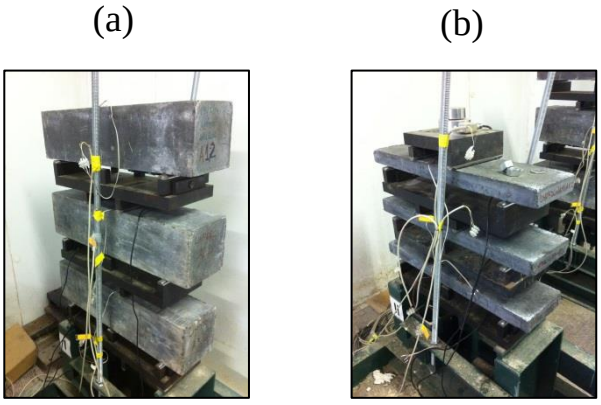

Figure 5. Multiple-specimen setup for flexural creep tests: (a) regular specimens, and (b) slim specimens.

3.3. Compressive creep tests

Compressive creep tests under sustained load were performed during 360 days. Three cylindrical UHPFRC specimens were tested in compressive creep following the methodology described in ASTM C512 [41] in a multiple-specimen setup, as shown in Fig. 6. In addition, one extra UHPFRC specimen was selected as reference for shrinkage stains, which was tested free of any load during the same time lapse than the compressive creep specimens. The stress applied to compressive creep specimens was 47.05 MPa, in correspondence to the desired stress level of 40% of f_c.

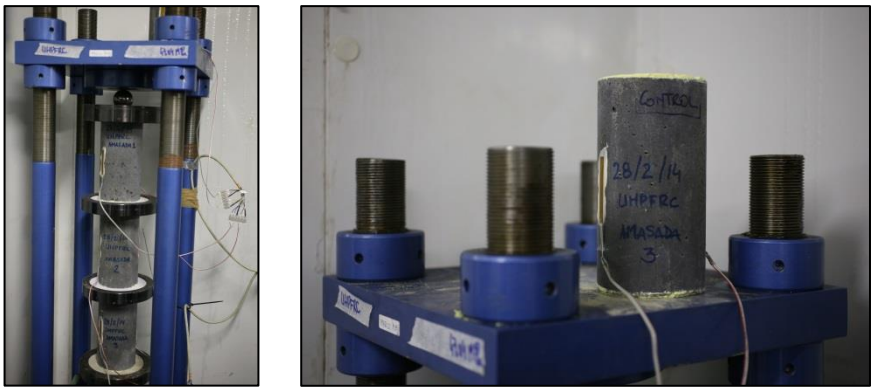

Figure 6. (a) Compressive creep test frame and (b) shrinkage specimen.

4. RESULTS AND ANALYSIS

4.1. Characterization tests

The concrete compressive strength at 28 days (f_c) was determined by testing four specimens. The average compressive strength was 117.6 MPa, with a coefficient of variation (CV) of 3.0%. Once the compressive creep tests were finished, the cylindrical specimens were tested in compression. The average compressive strength at the age of 441 days raised up to 135.64 MPa, with a CV of 6.7%.

In order to characterize the flexural behavior of the UHPFRC, three type R specimens were tested following EN14651:2007 [35]. The stress vs. CMOD curves obtained are shown in Fig. 7.

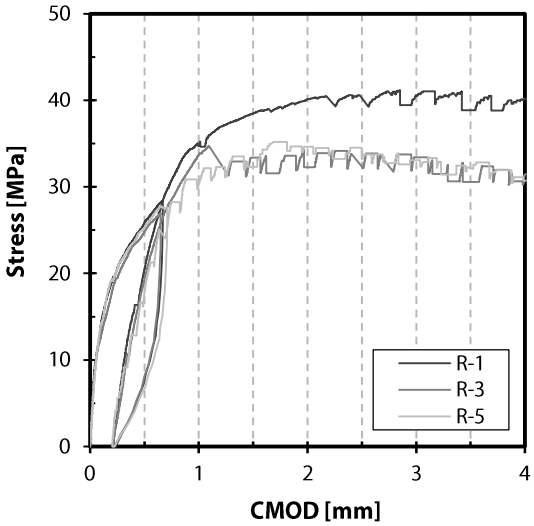

Figure 7. Results of flexural strength characterization tests.

All specimens presented similar Limit Of Proportionality (LOP, or f_L) and similar residual flexural tensile strength corresponding to $CMOD_1$ = 0.5 mm ($f_{R,1}$), as summarized in Table 4. The remaining residual strength parameters ($f_{R,2}$, $f_{R,3}$, and $f_{R,4}$, corresponding to CMOD values of 1.5, 2.5 and 3.5 mm, respectively), presented a slight scatter of results but not higher than a CV of 12.9%. As a result, following the classification of post-cracking behavior of FRC

according to Model Code 2010 [42], the tested UHPFRC can be denoted as "25e" with an average $f_{R,1}$ higher than 25 MPa and a residual strength ratio $f_{R,3}/f_{R,1}$ higher than 1.3.

Table 4. Residual flexural tensile strength (in MPa) for the tested UHPFRC according to EN14651:2007 [35].

Specimen	f_L	Residual strength					MC2010 Class.
		$f_{R,1}$	$f_{R,2}$	$f_{R,3}$	$f_{R,4}$	$f_{R,3}/f_{R,1}$	
R-1	9.48	25.84	38.46	40.61	38.85	1.57	25e
R-3	9.42	24.79	33.38	33.80	30.56	1.36	24e
R-5	9.42	25.26	32.29	33.23	32.26	1.32	25e
Average	*9.44*	*25.30*	*34.71*	*35.88*	*33.89*	*1.42*	*25e*
CV (%)	*0.40*	*2.1*	*9.5*	*11.4*	*12.9*	*9.6*	

4.2. Flexural creep tests: pre-cracking

Fig. 8 shows the [stress vs CMOD] curves of the pre-cracking stage for both regular and slim specimens. As observed in Fig. 8(a), $CMOD_p$ ranged from 0.67 to 0.72 mm in the case of type R specimens, which are near of the desired $CMOD_p$ of 0.65 mm specified in section 2.3. Also in Fig. 8(a), it is depicted that $CMOD_p$ ranged from 0.14 to 0.22 mm in the case of type S specimens, which resulted in a slight scatter in pre-crack level and, in turn, in stress level to be applied during the creep period. This is due to the adopted criterion to damage the type S specimens before the flexural creep test, which was applied in terms of specimen stiffness. As shown in Fig. 8(b), specimens type S were loaded until a 50% loss of the initial stiffness was observed, and this was performed simultaneously with the registration of the corresponding CMOD values.

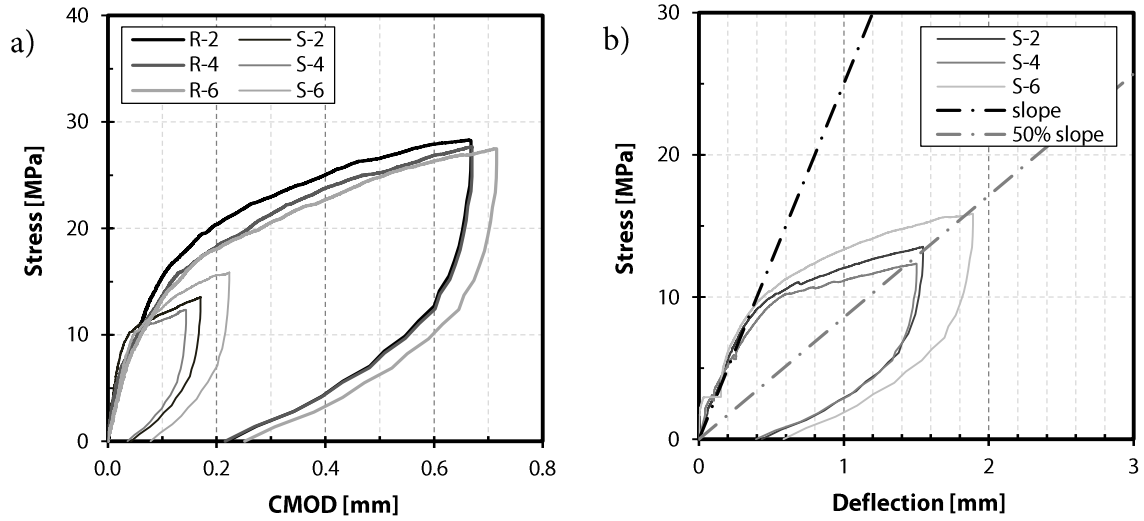

Figure 8. (a) Curves stress vs CMOD in the pre-cracking stage. (b) Pre-cracking criteria for slim specimens.

4.3. Flexural creep tests: creep period

During the flexural creep period, both the CMOD ─at the bottom of each specimen─ and the compressive strains (CS) ─on the top of specimens─ were measured and recorded. Fig. 9

shows the evolution in time of these parameters for all (types R and S) specimens. The depicted values correspond to the total effects due to loads (instantaneous and sustained), which were obtained from the values directly measured by accounting the shrinkage effect (the concrete shrinkage strains at each time j —$\varepsilon_{cs}{}^{j}$— is depicted in Fig. 13).

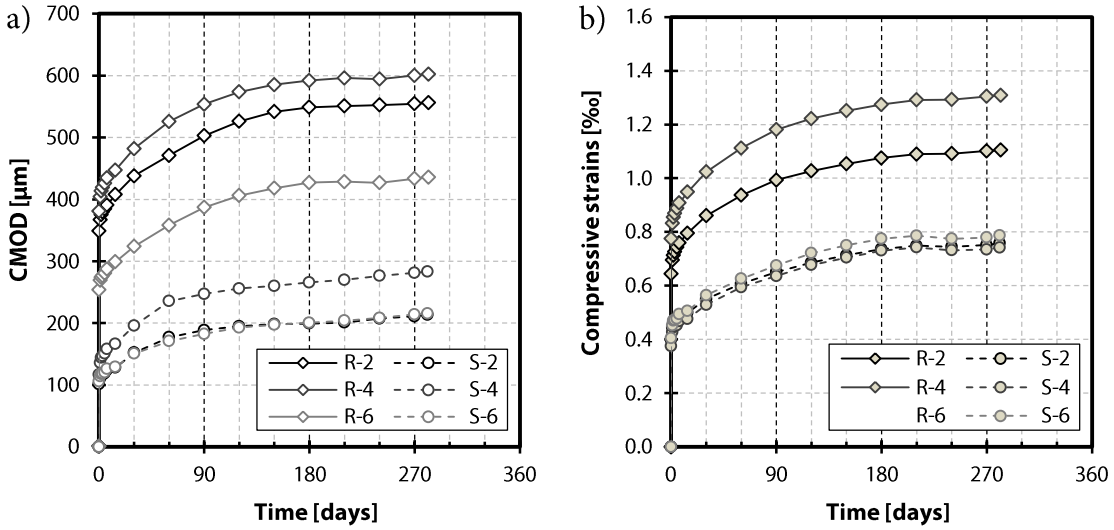

Figure 9. Test results in the flexural creep period: (a) CMOD [$CMOD_{ct}{}^{j}$], and (b) compressive strains [$CS_{ct}{}^{j}$].

As observed in Fig. 9, despite the inevitable dispersion of results, curves can be clearly grouped by type of specimen. Regarding CMOD (Fig. 9(a)): (a) specimens type R present instantaneous values ranging from 250 to 380 microns, whereas specimens type S present instantaneous values around 100 microns; (b) specimens type R present final values ranging from 400 to 600 microns, which implies deferred CMOD of 150-200 microns, whereas specimens type S present final values ranging from 200 to 260 microns, which implies deferred CMOD of 100-160 microns; and (c) specimens type S show lower scattered curves than specimens type R, as 2 specimens S-2 and S-6 present very similar results. Regarding CS (Fig. 9(b)): (a) specimens type R present instantaneous values ranging from 0.6‰ to 0.8‰, whereas specimens type S present instantaneous values around 0.4‰; (b) specimens type R present final values ranging from 1.2-1.4‰, which implies deferred CS around 0.6‰, whereas specimens type S present final values ranging around 0.85‰, which implies deferred CMOD around 0.45‰; and (c) all three specimens type S practically show the same behavior, whereas specimens type R (2 of them, as strain gauge of specimen R-6 failed) present the same relative position than in the case of CMOD curves, although with a wider span of values. The greater scatter of values in the case of specimens type R may be attributed to a more pronounced influence of micro-cracks due to the greater depth of the specimens.

There are significant parameters to be considered for analyzing the flexural concrete creep behavior, such as: (a) creep coefficients, defined as the ratio between the deferred and the initial values: and (b) parameters related with velocity of increase of deferred effects.

The CMOD creep coefficient at j days ($\varphi_{CMOD,c}{}^{j}$) can be obtained from CMOD measurements by means of Eq. (1):

$$\varphi_{CMOD,c}{}^{j} = CMOD_{cd}{}^{j} / CMOD_{ci} \quad (1)$$

where $CMOD_{cd}^{j}$ is the deferred CMOD ─obtained from the measured value by adding the shrinkage effect along the instrumented base length─ after j days under sustained load in the flexural creep period, and $CMOD_{ci}$ is the instantaneous CMOD at loading in the flexural creep period.

In a similar way, it can be also obtained the crack opening rate (COR) parameter which evaluates (in μm/year) the velocity of deferred crack opening occurrence in a certain lapse of time ─from day j to day k (COR^{j-k})─ by means of Eq. (2):

$$COR^{j-k} = (CMOD_{cd}^{k} - CMOD_{cd}^{j}) / ((k - j) / 365) \quad (2)$$

where $CMOD_{cd}^{j}$ and $CMOD_{cd}^{k}$ are the deferred CMOD ─again corrected by shrinkage─ after j and k days under sustained load, respectively, and j and k are time input data in days of the time lapse studied.

Table 5 summarizes the CMOD results for several time lapses selected for analysis purposes. In addition, to facilitate the understanding of readers, the creep coefficients according to Eq. (1) and the COR values from 240 to 270 days ($COR^{240-270}$) according to Eq. (2) have been included by way of example. All creep coefficients and COR values are depicted in Fig. 10, which shows the evolution in time of the creep coefficients for the selected time lapses and the COR values for a sequence of 30-day periods (the obtained COR is represented in the middle of the corresponding period).

Table 5. CMOD (in microns) at several time lapses in the flexural creep period.

Specimen	$CMOD_{ci}$	$CMOD_{ct}^{14}$	$CMOD_{ct}^{30}$	$CMOD_{ct}^{90}$	$CMOD_{ct}^{180}$	$CMOD_{ct}^{270}$	$\varphi_{CMOD,c}^{270}$	$COR^{240-270}$ (μm/year)
R-2	348.9	407.6	437.8	502.8	548.9	554.4	0.55	23.6
R-4	380.7	447.1	482.0	553.7	591.9	600.2	0.54	70.9
R-6	253.9	299.1	323.8	387.1	427.0	433.5	0.66	80.4
S-2	101.3	127.9	152.2	188.7	199.2	211.0	0.89	45.1
S-4	116.8	166.4	195.6	247.2	265.8	281.3	1.24	60.4
S-6	105.6	129.0	150.8	182.4	200.5	214.1	0.85	68.0

As observed in Fig. 10, curves can be clearly grouped by type of specimen. Regarding creep coefficients obtained according to Eq. (1), the average tendency for specimens type R leads to values around 0.62 at 270 days, as observed in Fig. 10(a), whereas the average tendency for specimens type S leads to mean values around 1.20. It should be noted that, although regular (R) specimens $CMOD_{ct}$ deformations are larger than slim ones, as shown in Fig. 9(a), slim (S) specimens present higher creep coefficients than regular ones. This effect is due to the differences in the instantaneous deformation ($CMOD_{ci}$), as shown in Fig. 11(a), since the required load to achieve the adopted creep index (I_c) is different for both specimens type, and also their stiffness. However, these differences in loads and stiffness between specimens did not affect the deferred behavior since the same I_c was applied, as observed in Fig. 11(b): $CMOD_{cd}$ deformations reached between 100 and 200 microns at 270 days regardless specimen type. Therefore, the instantaneous deformations became quite significant in the creep coefficients calculation since the $CMOD_{ci}$ location in Eq. (1) is in the denominator.

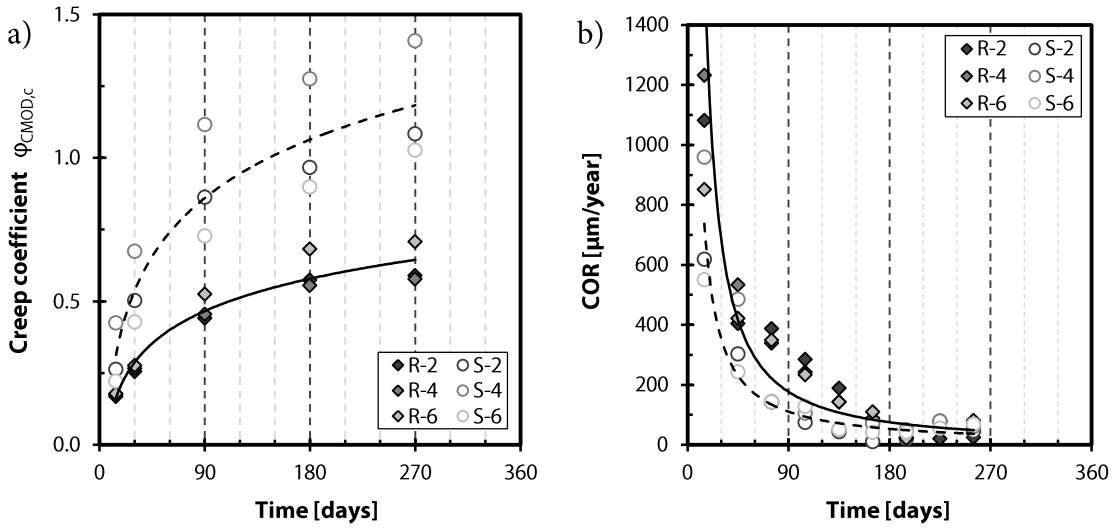

Figure 10. Parameters obtained from CMOD measurements: (a) creep coefficients [$\varphi_{CMOD,c}^{j}$], and (b) crack opening rate [COR^{j-k}, with k = j +30 and j = 0, 30, 60, …, 240].

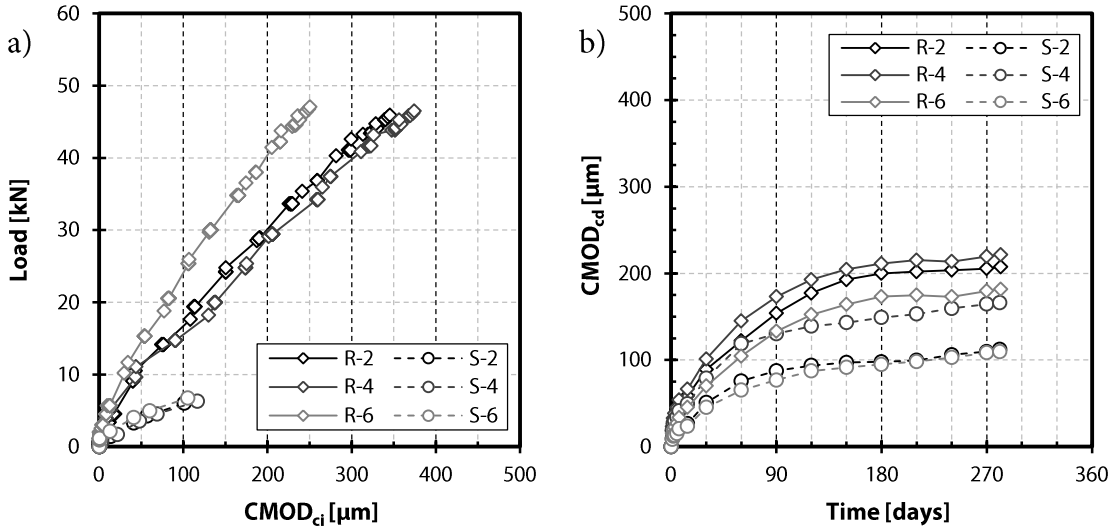

Figure 11. (a) Instantaneous deformations ($CMOD_{ci}$) and (b) deferred deformations ($CMOD_{cd}$) in flexural creep test.

Regarding COR values, as observed in Fig. 10(b), at early ages specimens type R present greater values than specimens type S, and all COR values tend to stabilize beyond 210 days.

Concerning measurements of compressive strains in flexural creep tests, Eq. (3) allows to calculate creep coefficients at different ages obtained from compressive strain measurements in the flexural creep period ($\varphi_{CS,c}^{j}$), as follows:

$$\varphi_{CS,c}^{j} = CS_{cd}^{j} / CS_{ci} \quad (3)$$

where CS_{cd}^{j} is the deferred concrete compressive strain after j days under sustained load in the flexural creep period ─obtained as the measured value minus ε_{cs}^{j}, which is concrete shrinkage strain at time j─, and CS_{ci} is the instantaneous compressive strain at loading in the flexural creep period.

Analogously, it can be also obtained the compressive strain rate (CSR) parameter which evaluates (in μstrains/year) the velocity of deferred concrete compressive strains occurrence in flexure in a certain lapse of time ─from day j to day k (CSR^{j-k})─ under sustained load in the flexural creep period by means of Eq. (4):

$$CSR^{j-k} = (CS_{cd}{}^{k} - CS_{cd}{}^{j}) / ((k - j) / 365) \quad (4)$$

where $CS_{cd}{}^{j}$ and $CS_{cd}{}^{k}$ are the deferred compressive strains corrected by shrinkage after j and k days under sustained load, respectively, and j and k are time input data in days which define the analyzed time lapse.

Table 6 summarizes the concrete compressive strain results in flexure for several time lapses selected for analysis purposes. In addition, to facilitate the understanding of readers, the creep coefficients according to Eq. (3) and the CSR values from 240 to 270 days ($CSR^{240-270}$) according to Eq. (4) have been included by way of example. All creep coefficients and CSR values are depicted in Fig. 12, which shows the evolution in time of the creep coefficients for the selected time lapses and the CSR values for a sequence of 30-day periods (the obtained CSR is represented in the middle of the corresponding period).

Table 6. Concrete compressive strains at several time lapses in the flexural creep period.

Specimen	CS_{ci}	$CS_{ct}{}^{14}$	$CS_{ct}{}^{30}$	$CS_{ct}{}^{90}$	$CS_{ct}{}^{180}$	$CS_{ct}{}^{270}$	$\varphi_{CS,c}{}^{270}$	$CSR^{240-270}$ (strains/year)
R-2	0.644	0.795	0.861	0.993	1.075	1.102	0.91	127.0
R-4	0.775	0.948	1.023	1.181	1.274	1.304	0.85	143.7
S-2	0.399	0.499	0.550	0.651	0.736	0.751	1.20	79.6
S-4	0.375	0.476	0.529	0.636	0.731	0.735	1.30	40.5
S-6	0.405	0.506	0.565	0.675	0.775	0.780	1.24	57.2

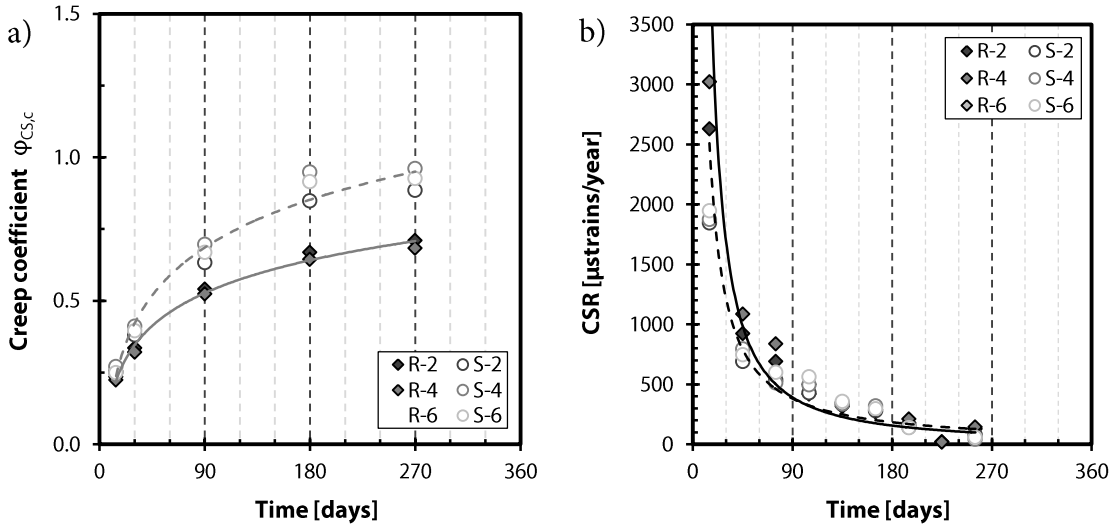

Figure 12. Parameters obtained from concrete compressive strains in the flexural creep period: (a) creep coefficients [$\varphi_{CS,c}{}^{j}$], and (b) compressive strain rate [CSR^{j-k}, with k = j +30 and j = 0, 30, 60, 90, …, 240].

As shown in Fig. 12, again curves can be grouped by type of specimen. It can be observed the same tendencies than in Fig. 10. As observed in Fig. 12(a), creep coefficient $\varphi_{CS,c}$ trends for both specimen types are closer than in the case of $\varphi_{CMOD,c}$ coefficients (see Fig. 10(a)), since

there is not such difference in the instantaneous deformations in compressive zone of the specimens during loading stage. Also, CS_{cd} reaches values around 0.0004-0.0005 at 270 days regardless specimen type, as deduced from Fig. 9(b). However, now the average tendency for specimens type R leads to values around 0.72 (instead of 0.62) at 270 days, whereas the average tendency for specimens type S leads to mean values around 0.90 (instead of 1.20). The differences in creep coefficients indicate that the creep phenomenon may develop in a different way in the tensile zone than in the compressive zone. Regarding the CSR evolution, it can be observed in Fig. 12(b) that the size and shape of the specimen is not significant, since the CSR follows the same trend path and velocity of propagation for both type of specimens. As in the case of COR parameter, at early ages specimens type R present greater CSR values than specimens type S, and CSR values also tend to stabilize beyond 210 days.

4.4. Long-term tests on cylindrical specimens: compressive creep and shrinkage

For the analyzed period, concrete strains from both loaded (creep in compression) and unloaded (shrinkage) specimens were measured and recorded. Fig. 13 shows the evolution in time of these strains. For specimens C-2, C-4 and C-7, the depicted values correspond to the total concrete compressive strains at time j due to load during creep test in compression ($\varepsilon_{ct}{}^{j}$), which include the instantaneous strain (ε_{ci}) and the deferred strains at the time j ($\varepsilon_{cd}{}^{j}$). These values were obtained from the values directly measured by subtracting the corresponding concrete shrinkage strain at time j ($\varepsilon_{cs}{}^{j}$), which are also depicted in Fig. 13 for specimen SR-8. As observed in Fig. 13, all three specimens tested in compression present similar results, and the shrinkage deformations at one year loading represent the 5.7% of the total deformations under compressive constant load.

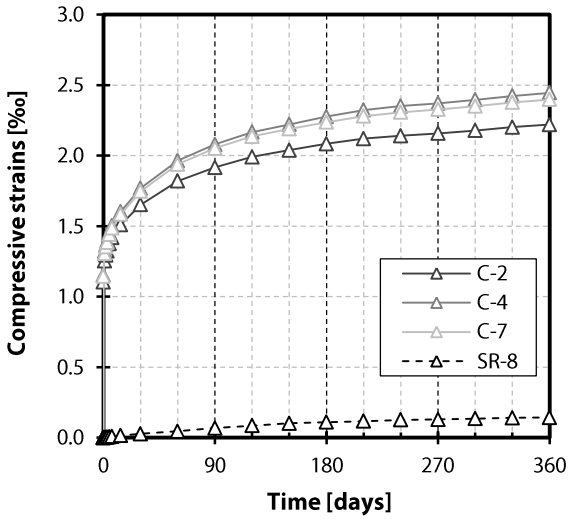

Figure 13. Test results from creep in compression test: concrete compressive strains [$\varepsilon_{ct}{}^{j}$] for specimens C-2, C-4 and C-7, and concrete shrinkage strains [$\varepsilon_{cs}{}^{j}$] for specimen SR-8.

As done for the case of flexural creep, there are significant parameters to be considered for analyzing the concrete creep behavior in compression. The creep coefficients at j days in compression (φ^{j}) can be obtained by Eq. (5):

$$\varphi^{j} = \varepsilon_{cd}{}^{j} / \varepsilon_{ci} \quad (5)$$

where $\varepsilon_{cd}^{\ j}$ is the deferred ε_c after j days under sustained load in compression ─obtained as the measured value minus $\varepsilon_{cs}^{\ j}$, which is concrete shrinkage strain at time j─ and ε_{ci} is the instantaneous ε_c at loading in compression.

The compressive strain rates in compressive creep test between j and k days (CR^{j-k}) are defined (in μstrains/year) by Eq. (6), as follows:

$$CR^{j-k} = (\varepsilon_{cd}^{\ k} - \varepsilon_{cd}^{\ j}) / ((k - j) / 365) \quad (6)$$

where $\varepsilon_{cd}^{\ j}$ and $\varepsilon_{cd}^{\ k}$ are the deferred ε_c after j and k days, respectively, under sustained load in compression as previously defined, and j and k are time lapse input data in days.

Table 7 summarizes the concrete strains results in compression for several time lapses selected for analysis purposes. In addition, to facilitate the understanding of readers, the creep coefficients according to Eq. (5) and the CR values from 240 to 270 days ($CR^{240-270}$) according to Eq. (6) have been included by way of example. All creep coefficients and CR values are depicted in Fig. 14, which shows the evolution in time of the creep coefficients for the selected time lapses and the CR values for a sequence of 30-day periods (the obtained value is represented in the middle of the corresponding period). As observed in Fig. 14(a), all three specimens tested under compression present similar results for both parameters. After one year, the creep coefficient is 1.07, whereas at 270 days, just when the flexural creep test was stopped, creep coefficient is around 1. Regarding the CR parameter, the general trend coincides with the case of COR and CSR parameters, with a constant value beyond 210 days as it can be observed in Fig. 14(b), which indicates that the secondary creep stage is achieved.

Table 7. Concrete compressive strains at several time lapses in creep in compression.

Specimen	ε_{ci}	ε_{ct}^{14}	ε_{ct}^{30}	ε_{ct}^{90}	ε_{ct}^{180}	ε_{ct}^{270}	ε_{ct}^{360}	φ^{270}	φ^{360}	$CR^{240-270}$ (μstrains/year)
C-2	1.104	1.511	1.652	1.917	2.084	2.158	2.220	0.95	1.01	215.8
C-4	1.153	1.603	1.769	2.080	2.277	2.371	2.446	1.06	1.12	229.6
C-7	1.144	1.584	1.748	2.052	2.238	2.328	2.399	1.03	1.10	245.0
SR-8	0.001	0.015	0.027	0.069	0.110	0.129	0.142	--	--	--

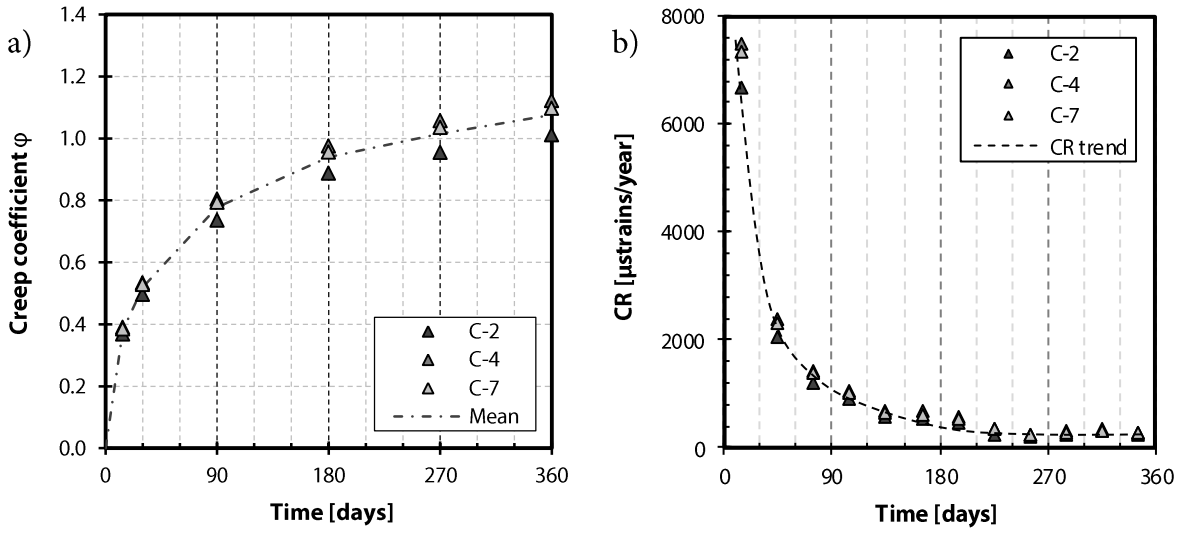

Figure 14. Parameters obtained from creep in compression test: (a) creep coefficients (φ^{j}), and (b) CR^{j-k}, where k = j +30 and j = 30, 60, 90, …, 330.

4.5. Comparison of creep coefficients

Comparing to the reference creep coefficients obtained in compression test, the flexural creep coefficients differ depending on the type specimen, as shown in Fig. 15. Whereas creep coefficients of specimens type S from both CMOD and CS measurements are close to the reference creep coefficients (Fig. 15(b)), specimens type R give creep coefficients around 30% smaller than the reference (Fig. 15(a)). This fact can be explained from the differences registered in the instantaneous deformation ($CMOD_{ci}$ and CS_{ci}), which are greater in the case of specimens type R and this results in lower creep coefficients according to Eq. (1) and Eq. (2).

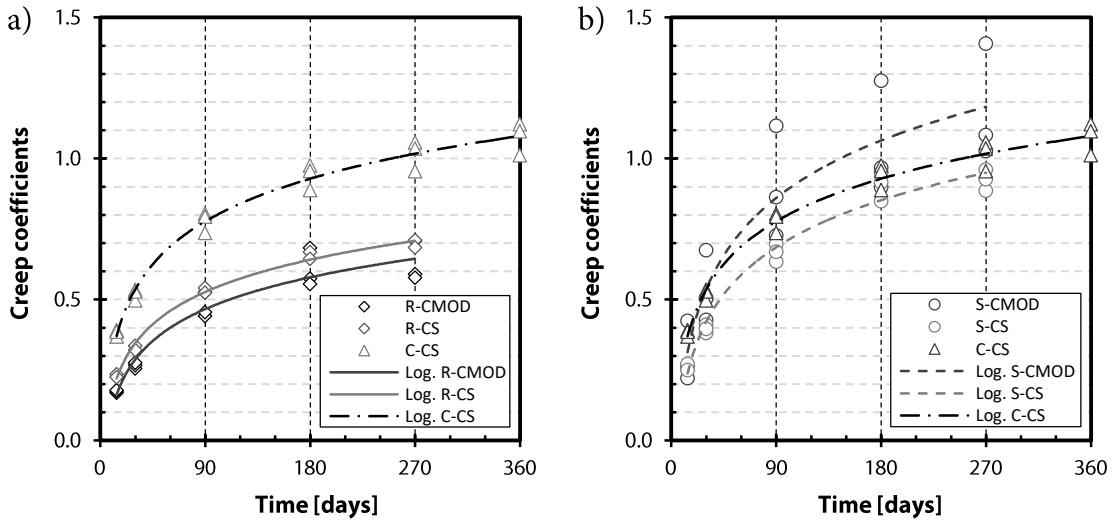

Figure 15. Comparison of creep coefficients obtained in (a) regular specimens, and (b) slim specimens.

In addition, the creep coefficient $\varphi_{CS,c}$ for specimens type R is slightly higher than the $\varphi_{CMOD,c}$ creep coefficient, which means that for this type of prismatic specimen the creep in the compressive zone seems to be more significant than the creep in the tensile zone. On the contrary, for the specimens type S, $\varphi_{CMOD,c}$ values are higher than $\varphi_{CS,c}$, which implies that in case of slim specimens the creep in the tensile zone seems to be more significant in deferred behavior. The different configuration of cracks, that is, discrete cracks induced and located at the notch tip in the case of specimens type R, and distributed micro-cracks along the tensile base length measured in specimens type S, together the different effectiveness of the fibers (short and long fibers) bridging cracks, have to be taken into account in order to explain these facts, as follows: (a) the shortest fibers control the micro-cracks, and a progressive loss of effectiveness bridging cracks occurs while the contribution of the longest fibers is not activated; and (b) the longest fibers control the macro-cracks, and the activation of their forces bridging cracks results more effective and implies the concrete creep in the compressive zone is more pronounced.

In general terms, the obtained creep coefficients are consistent with values presented in Table 1: between 0.78 [24] and 1.20 for standard cure regime (for date of loading of 28 days [23] or regardless that date [22]). As aforementioned, the concrete tested represent an unfavourable case, which explains that the obtained values (1.01 to 1.12) of creep coefficient at 360 days in compression (φ^{360}) are greater than 0.78 (creep coefficient at one year of loading) and slightly smaller than 1.20 (which is a final creep coefficient).

4.6. Comparison of deformation rate parameters in compression

As compressive strain evolution was registered in time in both flexural and compressive creep tests in all the specimens, a comparison can be performed in order to analyze the deformation rate differences between methodologies. Fig. 16 depicts the CSR and CR parameters for all specimens and their corresponding potential fitting curve.

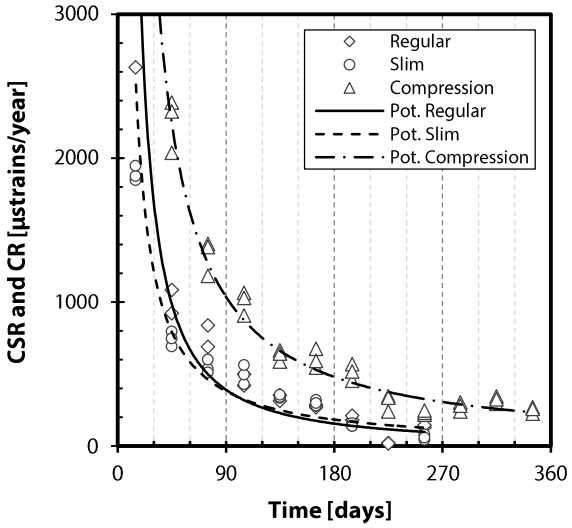

Figure 16. Comparison of compressive strains rates CSR and CR for all specimens.

As observed in Fig. 16, despite the differences found between the two types of specimens in creep coefficients evolution, both types followed similar potential trends regarding the CSR parameter. That means that the creep deformations corresponding to the compressive zone of the flexural schema increased with the same velocity for both the regular and for slim specimens. This can be explained based on the absence of cracks in the compressive zones, which reflect the concrete behavior and not the different contribution of the shortest and longest fibers as occurred in the case of the tensile zones. On the other hand, CR values were greater than those of CSR mainly at early ages, which can be considered due to the uniformity in compressive stresses in the case of cylindrical specimens with regard to a linear distribution in the case of prismatic specimens, and also present a stabilization tendency beyond 210 days.

5. CONCLUSIONS

The long term behavior of UHPFRC specimens under several creep test conditions has been analyzed in this work. Creep in compression and flexural creep tests have been developed on specimens having different size and shape, and measurements from three experimental sources have allowed obtaining creep coefficients and parameters related with deferred deformations velocity. The following conclusion can be drawn:

- Differences in stiffness between specimens have not affected the deferred behavior in the cracked state under flexure. At 270 days, $CMOD_{cd}$ deformations ranging between 100 and 200 microns and CS_{cd} values around 0.0004-0.0005 were achieved regardless specimen type.

- Creep coefficients under flexure at 270 days were different based on specimen type. In the tensile zone: 0.62 for regular specimens and 1.20 for slim specimens. In the compressive zone: 0.72 for regular specimens and 0.90 for slim specimens. Differences based on type of specimens can be explained from the different procedure applied regarding the initial damage at pre-cracking, whereas differences between zones ─tensile and compressive zones of a same specimen─ indicate that the creep phenomenon may develop in a different manner in the cracked state due to a redistribution of stresses along the cross sections.
- In the case of specimens type S, the creep in the tensile zone seems to be more significant than the creep in the compressive zone, as a progressive loss of effectiveness of the shortest fibers bridging cracks occurs while the contribution of the longest fibers is not activated. In the case of specimens type R, the creep in the compressive zone seems to be more significant than the creep in the tensile zone, as discrete cracks induced and located at the notch tip activate the contribution of the longest fibers in an effective manner which implies the concrete creep in the compressive zone is more pronounced.
- Regarding the parameters related with velocity of increase of deferred deformation in flexure, the size and shape of the specimen have been not significant, since both the COR and the CSR followed the same trend path and velocity of propagation for both type of specimens. At early ages specimens type R presented greater COR and CSR values than specimens type S, and in all cases COR and CSR parameters tended to stabilize beyond 210 days.
- Creep coefficient in compression was around 1 at 270 days, just when the flexural creep test was stopped, which was close to the creep coefficients obtained from specimens type S. And at one year, creep coefficient in compression was 1.07, which is consistent with some values found in the literature.
- Regarding the parameter related with velocity of increase of deferred deformation in compression, CR always presented higher values than CSR and depicted the same trend than COR and CSR parameters, with a constant value beyond 210 days which indicates that the secondary creep stage was achieved.

ACKNOWLEDGMENTS

The authors wish to thank the technicians of ICITECH, where the experimental work was developed. The financial support of the project BIA2016-78460-C3-1-R “Bases para el diseño de estructuras sostenibles de hormigón de muy alto rendimiento a nivel prenormativo / Diseño eficiente de estructuras de HMAR”, supported by the Spanish Ministry of Economy and Competiveness and the FEDER funds, is also gratefully acknowledged.

REFERENCES

[1] Portland Cement Association, https://www.cement.org/learn/concrete-technology/concrete-design-production/ultra-high-performance-concrete, Consultation on 01/11/2018.
[2] F. de Larrard, T. Sedran, Optimization of Ultra-High-Performance Concrete by the use of a packing model, Cem. Concr. Res. 24 (6) (1994) 997–1009.
[3] B. Graybeal, Ultra-high-performance concrete connections for precast concrete bridge decks, PCI J. 49 (4) (2014) 48–62.

[4] A. Alsalman, C.N. Dang, J.R. Martí-Vargas, W. M. Hale, Mixture-proportioning of economical UHPC mixtures, J. Build. Eng. 27 (2020) 100970.
[5] A. Naaman A, High performance fiber reinforced cement composites. In: Proceedings of the IABSE symposium on concrete structures for the future, 1987, pp 371–376.
[6] E. Denarié, E. Brühwiler, Cast-on site UHPFRC for improvement of existing structures – achievements over the last 10 years in practice and research. Proceedings of the 7th RILEM Workshop on High Performance Fiber Reinforced Cement Composites. 2015. Pp. 473–480.
[7] R. Adeline, M. Lachemi, P.Y. Blais, Design and behaviour of the Sherbrooke footbridge. Proceedings of the International Symposium on High Performance and Reactive Powder Concretes. Sherbrooke University, 1998, pp. 59–63.
[8] B. Moore, D. Bierwagen, Ultra-High Performance Concrete Highway Bridge", Portland Cement Association, 2006.
[9] M. Reichel, B. Freytag, L. Sparowitz, Road Bridge WILD-UHPFRC for a segmental arch structure. BFUP 2009/UHPFRC 2009 Proceedings.
[10] J.A. López, P. Serna, P., E. Camacho, H. Coll, J. Navarro-Gregori, First ultra-high-performance fibre-reinforced concrete footbridge in spain: design and construction, Struct. Eng. Int. 24 (1) (2014) 101–104.
[11] J. Walraven J. High performance fiber reinforced concrete: progress in knowledge and design codes, Mater. Struct. 42 (2009) 1247–1260.
[12] Federal Highway Administration (FHWA), Publication No. FHWA-HRT-13-060 Ultra-High Performance Concrete: A State-of-the-Art Report for the Bridge Community. 2013.
[13] G.Y. Kim, J.H. Choi, S.E. Park, H. Kim, Y. Le, B.Y. Lee, Response of UHPFRC and HDFRC under static and high-velocity projectile impact loads, Constr. Build. Mat. 188 (2018) 399–408.
[14] P.A. Krahl, G. Saleme, R. Carrazedo, Compressive behavior of UHPFRC under quasi-static and seismic strain rates considering the effect of fiber content, Constr. Build. Mat. 188 (2018) 633–644.
[15] Ch. Kahanji, F. Ali, A. Nadjai, N. Alam, Effect of curing temperature on the behaviour of UHPFRC at elevated temperatures, Constr. Build. Mat. 182 (2018) 670–681.
[16] M. Foglar, R. Hajek, J. Fladr, J. Pachman, J. Stoller, Full-scale experimental testing of the blast resistance of HPFRC and UHPFRC bridge decks, Constr. Build. Mat. 145 (2017) 588–601.
[17] N. Buratti, C. Mazzotti, M. Savoia, Post-cracking behaviour of steel and macro-synthetic fibre-reinforced concretes, Constr. Build. Mat. 25 (2011) 2713–2722.
[18] J.A. López, P. Serna, J. Navarro-Gregori, E. Camacho, An inverse analysis method based on deflection to curvature transformation to determine the tensile properties of UHPFRC, Mater. Struct. 48(11) (2015) 3703–3718.
[19] W. Li, Z. Huang, G. Hu, W.H. Duan, S.P. Shah, Early-age shrinkage development of ultra-high-performance concrete under heat curing treatment, Constr. Build. Mat. 131 (2017) 767–774.
[20] Y. Xu, J.P. Liu, J.Z. Liu, P. Zhang, Q.Q. Zhang, L.H. Jiang, Experimental studies and modeling of creep of UHPC, Constr. Build. Mat. 175 (2018) 643–652.
[21] Association Française de Genie Civil (AFGC), Ultra-High Performance Fiber Reinforced Concretes. Recommendations, 2013.
[22] Japanese Society of Civil Engineers (JSCE), Recommendations for Design and Construction of Ultra High Strength Fiber Reinforced Concrete Structures (Draft). Subcommittee on Research of Ultra High Strength Fiber Reinforced Concrete. 2006. Tokyo, Japan

[23] N. Gowripalan, R.L. Gilbert, Design Guidelines for RPC Prestressed Concrete Beams, VSL (Australia) Pty Ltd, 2000.
[24] B. Graybeal, Material Property Characterization of Ultra-High Performance Concrete, Federal Highway Administration, Office of Research, Development and Technology, Turner-Fairbank Highway Research Center, 2006.
[25] G. Plizzari, P. Serna, Structural effects of FRC creep, Mater. Struct. 51 (2018) 167
[26] V.Y. Garas, L.F. Kahn, K.E. Kurtis, Short-term tensile creep and shrinkage of ultra-high performance concrete, Cem. Concr. Comp. 31 (2009) 147–152.
[27] A. Kamen, E. Denarié, H. Sadouki, E. Brühwiler, UHPFRC tensile creep at early age, Mater. Struct. 42 (1) (2009) 113–122.
[28] A. Switek-Rey, E. Denarie, E. Bruhwiler, Early age creep and relaxation of UHPFRC under low to high tensile stresses, Cem. Concr. Res. 83 (2016) 57–69.
[29] V.Y. Garas, K.E. Kurtis, L.F. Kahn, Creep of UHPC in tension and compression: Effect of thermal treatment, Cem. Concr. Comp. 34 (2012) 493–502.
[30] D. Casucci, Tensile creep in ultra-high-strength fiber-reinforced concrete (UHPFRC): Experimental Investigation on cracked tensile specimens, Beton und Stahlbetonbau 112 (7) (2017) 440–440.
[31] D. Casucci, C. Thiele, J. Schnell, Behavior of cracked cross-section of fibre reinforced UHPFRC under sustained load. Proceedings of the International RILEM Workshop FRC-CREEP 2016 "Creep Behaviour in Cracked Sections of Fibre Reinforced Concrete", Valencia, 2016, RILEM Bookseries 14, Eds. Serna, P, Cavalaro, S. and Llano-Torre, A. ISBN 978-94-024-1000-6.
[32] E. Galeote, A. Blanco, A. de la Fuente, S.H.P. Cavalaro, Creep behaviour of cracked high performance fibre reinforced concrete beams under flexural load. Proceedings of the International RILEM Workshop FRC-CREEP 2016 "Creep Behaviour in Cracked Sections of Fibre Reinforced Concrete", Valencia, 2016, RILEM Bookseries 14, Eds. Serna, P, Cavalaro, S. and Llano-Torre, A. ISBN 978-94-024-1000-6.
[33] T. Nishiwaki, S. Kwon, H. Otaki, G. Igarashi, F.UA. Shaikh, A.P. Fantilli, Experimental study on time-dependent behavior of cracked UHP-FRCC under sustained loads. Proceedings of the International RILEM Workshop FRC-CREEP 2016 "Creep Behaviour in Cracked Sections of Fibre Reinforced Concrete", Valencia, 2016, RILEM Bookseries 14, Eds. Serna, P, Cavalaro, S. and Llano-Torre, A. ISBN 978-94-024-1000-6.
[34] European Committee for Standardization, European Standard EN179-1:201, Cement - Part 1: Composition, specifications and conformity criteria for common cements, Brussels, 2011.
[35] European Committee for Standardization, European Standard EN 14651:2007: Test method for metallic fibered concrete - Measuring the flexural tensile strength (limit of proportionality (LOP), residual), Brussels, 2007.
[36] European Committee for Standardization, European Standard EN 12390-3:2009, Testing hardened concrete - Part 3: Compressive strength of test specimens, Brussels, 20097.
[37] S.E. Arango, P. Serna, J.R. Martí-Vargas, E. García-Taengua, A test method to characterize flexural creep behaviour of pre-cracked FRC specimens, Exp. Mech. 52(8) (2012) 1067–1078.
[38] E. García-Taengua, S. Arango, J.R. Martí-Vargas, P. Serna, Flexural creep of steel fiber reinforced concrete in the cracked state, Constr. Build. Mat. 65 (2014) 321–329.
[39] P. Serna Ros, J.R. Martí-Vargas, J.R., M.E. Bossio, R. Zerbino, Creep and residual properties of cracked macro-synthetic fibre reinforced concretes, Mag. Concr. Res. 68(4) (2016) 197–207.

[40] D.H. Monetti, A. Llano-Torre, M.C. Torrijos, G. Giaccio, R. Zerbino, J.R. Martí-Vargas, P. Serna, Long-term behavior of cracked fiber reinforced concrete under service conditions, Constr. Build. Mat. 196 (2019) 649–658.
[41] ASTM C512 / C512M-15, Standard Test Method for Creep of Concrete in Compression, American Society for Testing and Materials, West Conshohocken, PA, 2015.
[42] Fédération Internationale du Béton, fib Model Code for Concrete Structures 2010. Ernst & Sohn, Berlin, 2013, pp. 74–150.